



# Chemical looping capabilities of olivine, used as a catalyst in indirect biomass gasification



R.J. Lancee<sup>a,\*</sup>, A.I. Dugulan<sup>b</sup>, P.C. Thüne<sup>a</sup>, H.J. Veringa<sup>a,c</sup>, J.W. Niemantsverdriet<sup>a</sup>, H.O.A. Fredriksson<sup>a,\*</sup>

<sup>a</sup> Laboratory for Physical Chemistry of Surfaces, Eindhoven University of Technology, P.O. Box 513, 5600 MB Eindhoven, The Netherlands

<sup>b</sup> Fundamental Aspects of Materials and Energy Group, Delft University of Technology, Mekelweg 15, 2629 JB Delft, The Netherlands

<sup>c</sup> Department of Mechanical Engineering, Eindhoven University of Technology, P.O. Box 513, 5600 MB Eindhoven, The Netherlands

## ARTICLE INFO

### Article history:

Received 15 October 2012

Received in revised form 23 January 2013

Accepted 24 January 2013

Available online 31 January 2013

### Keywords:

Olivine

Biomass gasification

Chemical looping

Oxygen transport

Thermo gravimetric analysis

## ABSTRACT

Indirect biomass gasification systems consist of two reactors: an oxidation reactor and a gasification reactor. A bed-material is used to transfer heat from the oxidation to the gasification reactor. Olivine has been widely studied as a reactive bed-material for this process. The iron in olivine can act as a catalyst for the decomposition of tars, produced during the gasification process. Moreover, iron is capable of transferring oxygen to the gasification reactor. In this study, we elucidate the role of iron in this chemical looping process. Mössbauer spectra show that during oxidation in O<sub>2</sub>/Ar at 750 °C, iron segregates out of the olivine matrix forming free iron oxide phases. These free iron phases form metallic iron upon subsequent reduction in hydrogen. Thermo gravimetric analysis (TGA) is used to quantify oxygen transport under alternating oxidizing/reducing conditions. TGA results indicate that at least 18% of all the iron, present in olivine, is capable of transferring oxygen on the time scale of minutes. X-ray photoelectron spectroscopy (XPS) combined with depth profiling provides insight in the dynamic behavior of olivine under relevant conditions. Iron enrichment at the surface is observed; oxidized olivine has an iron rich surface layer of 400 nm. The increased iron concentration is particularly pronounced at the outermost surface. Upon subsequent reduction, the iron quickly redistributes in the olivine toward the original, homogeneous distribution. These results show that oxygen transport should be taken into account when olivine is evaluated as a catalyst for indirect biomass gasification. Furthermore, both oxygen transport and catalytic properties are heavily dependent on the iron phases present in the material, which in turn depend on the gas environment.

© 2013 Elsevier B.V. All rights reserved.

## 1. Introduction

To meet the increasing demand for renewable, CO<sub>2</sub>-neutral energy, biomass (in particular waste products) can be used for the production of such fuels as hydrogen, synthetic natural gas or Fischer-Tropsch diesel [1,2]. Conversion of biomass to fuels can be performed using the gasification process as an initial step in the conversion [3,4]. The resulting primary products CO, H<sub>2</sub>, CO<sub>2</sub> and CH<sub>4</sub> can easily be used in the present infrastructure. Moreover, technology for converting CO and H<sub>2</sub> into conventional fuels, such as diesel, is already at hand [5].

The endothermic gasification process is sustained by allowing partial combustion of the biomass, usually using air. If the heat required for the endothermic gasification is not supplied by partial combustion in the gasifier section, but instead comes from a

separate combustion step, which may be integrated in the gasification system, one speaks of indirect gasification. The main advantages of indirect gasification are the higher heating value of the produced gas, no N<sub>2</sub> contamination of the product gas and that a major part of the CO<sub>2</sub> produced in the process is separated from the product gases, allowing for sequestration.

In a typical indirect gasification system, a bed material is circulated between an oxidation reactor and a gasification reactor, coupled together. In the latter, biomass reacts with steam and is converted to a gas mixture consisting mainly of methane, synthesis gas and CO<sub>2</sub>. The bed-material, together with the unconverted biomass fractions, tar and char, are fed into the oxidation reactor, to heat up the bed material. The hot bed material subsequently enters into the gasification zone to provide the heat, necessary for gasification. In addition to the main product gases, the gasification process always results in tar formation due to incomplete decomposition of the biomass. Tars decrease process efficiency and can cause fouling of downstream equipment. This constitutes a major obstacle in the way to large scale commercialization of the technique.

\* Corresponding authors. Tel.: +31 40 247 4658; fax: +31 40 247 3481.

E-mail addresses: [R.J.Lancee@tue.nl](mailto:R.J.Lancee@tue.nl) (R.J. Lancee), [H.O.A.Fredriksson@tue.nl](mailto:H.O.A.Fredriksson@tue.nl) (H.O.A. Fredriksson).

Tar in the product gas can be decreased by using a reactive bed material [6–10]. A widely used and investigated bed material is the naturally occurring mineral olivine ( $(\text{Mg}, \text{Fe})_2\text{SiO}_4$ ) [11–14], in which iron is the catalytically active component for tar conversion [15–19]. Olivine is, however, not a stable material under process conditions, relevant for biomass gasification [14,20]. It has been shown that iron in olivine is highly mobile under alternating oxidizing and reducing environments [12]; iron enrichment at the surface is observed upon oxidation, whereas a decreased content is seen upon reduction [21]. Furthermore, the iron in olivine is oxidized in the oxidation zone and reduced in the gasification zone, and is thereby able to transport oxygen to the gasification zone. Oxygen transport lowers the necessary amount of steam for the gasification and increases tar degradation and fuel conversion [16,22], but it also (unwantedly) increases the  $\text{CO}_2$  content in the gasification zone.

This work focuses on the role of iron in the chemical looping process. When olivine is used as a circulating bed material, it is sequentially exposed to different gas environments on time scales from a few seconds to several minutes. Changes in the gas environment influence the phase composition of olivine in general, and the surface concentration and oxidation state of iron in particular. The dynamics of these effects have not been well documented yet. With this paper, we aim at clarifying the time dependent changes in olivine (and especially the Fe-components contained therein) in rapidly changing, yet well-defined, chemical environments.

We have used Mössbauer spectroscopy to determine the distribution of different iron species in olivine after oxidation and reduction treatments. Furthermore, we present thermo gravimetric analysis (TGA) as a valuable characterization tool to quantify oxygen transport of olivine, since exact figures or relations to quantify the amount of this transported oxygen are unknown. To get detailed information on the dynamic behavior of iron at the surface and sub-surface layers under oxidizing and reducing conditions, we use X-ray photoelectron spectroscopy (XPS) combined with depth profiling.

## 2. Experimental

### 2.1. Catalyst material and treatments

For all experiments, natural olivine from Magnolithe GmbH was used. A 3 h, 1600 °C calcination in air was performed by the mineral supplier to improve its mechanical properties. The grain size during this pre-calcination was on the order of 10 mm. The composition of this olivine is well-known and extensively documented [7,12,13]. The iron content of our olivine sample was determined by ICP-AES to be 6.3 wt.%.

Prior to our experiments, the olivine was grinded to a powder with grain sizes of several micrometers, as estimated from scanning electron microscopy (SEM) images. The olivine powder has a specific surface area of  $0.53 \text{ m}^2/\text{g}$  [23]. This grinded olivine will be denoted as “untreated” in this paper.

The grinded olivine powders were treated in a quartz tube flow reactor. Oxidation (20%  $\text{O}_2$  in Ar) and reduction (pure  $\text{H}_2$ ) treatments were applied at 750 °C. Total gas flows were set to 200 mL/min. In all experiments, the samples were first heated to 750 °C under pure Ar flow. At this temperature, the gas flow was switched to the reactive gas mixtures for a specified time. After treatment, the gas mixture was switched back to Ar and the reactor was quickly cooled to room temperature.

### 2.2. Mössbauer spectroscopy

Transmission  $^{57}\text{Fe}$  Mössbauer spectra were collected at room temperature with a conventional constant-acceleration spectrometer using a  $^{57}\text{Co}(\text{Rh})$  source. Velocity calibration was carried out using an  $\alpha$ -Fe foil. The Mössbauer spectra were fitted using the Mosswinn 3.0i program [24].

### 2.3. Thermo gravimetric analysis

Thermo gravimetric analysis (TGA) is a commonly used technique for studying reactive gas–solid systems. For measurements, the grinded, untreated olivine sample (200 mg) was placed in a porous quartz glass sample holder, connected by a platinum wire to a Sartorius 4406 balance, which measured the mass change of the sample during treatment. Gas treatments (oxidation (air, 8 mL/min) and reduction (30%  $\text{H}_2/\text{N}_2$ , 8 mL/min)) were applied at 750 °C in a home-built set-up, which is described in more detail elsewhere [25]. In between the oxidation and reduction treatment, the system was flushed with  $\text{N}_2$  for 1 min to prevent direct contact between  $\text{H}_2$  and  $\text{O}_2$ .

### 2.4. X-ray photoelectron spectroscopy

In this study, X-ray photoelectron spectroscopy (XPS) was combined with depth profiling. An ion gun was used to etch the sample's surface for a period of time before being turned off while XPS spectra were measured. Each etch step exposes a new surface and, by fitting the measured XPS spectra, the elemental concentrations at that specific surface could be determined. The objective of these experiments was to plot the trend in the atomic concentration values as a function of etch-time, or sample depth.

Olivine powder samples were supported on conductive carbon tape. XPS spectra were recorded using a Thermo Scientific K-Alpha spectrometer equipped with a monochromatic small-spot X-ray source and a 180° double focusing hemispherical analyzer with a 128-channel detector. Spectra were obtained using an aluminum anode ( $\text{Al K}\alpha$ , 1486.6 eV) operating at 72 W and a spot size of 400  $\mu\text{m}$ .

Region scans were measured at a constant pass energy of 50 eV. The background pressure was  $2 \times 10^{-9}$  mbar and during measurement  $3 \times 10^{-7}$  mbar argon, because of the charge compensation dual beam source.

Sputtering for depth profiling was done with an  $\text{Ar}^+$  ion beam energy of 2000 eV at medium current (12  $\mu\text{A}$ ). The ion gun was used for 120 s for each etch step, corresponding to a total depth per etch level of 37.2 nm for a  $\text{Ta}_2\text{O}_5$  reference.

Analysis and quantification of the measurements were performed using the CasaXPS software, using the Fe 3p, Mg 2p, Si 2p and O 1s regions.

## 3. Results

### 3.1. Mössbauer spectroscopy

Mössbauer spectroscopy was used to quantify the changes in the iron (oxidation) state of the olivine upon oxidizing and reducing treatments. The fitted spectra are presented in Fig. 1. The detailed fitting parameters and spectral contribution of the different iron species are presented in Table 1.

Fitting of the spectra in Fig. 1 required the use of two doublets and four sextuplets. The two doublets are attributed to  $\text{Fe}^{2+}$  in the olivine phase (D1) and  $\text{Fe}^{3+}$  in superparamagnetic hematite (D2), respectively [20]. Of the four sextuplets, the first two (S1 and S2) are identified as belonging to  $\text{Fe}^{3+}$  in octahedral and tetrahedral sites of the spinel structure of magnesioferrite ( $\text{MgFe}_2\text{O}_4$ ) [12,26].

**Table 1**

Mössbauer parameters of the olivine samples, obtained by fitting.

	IS (mm/s)	QS (mm/s)	Hyperfine field (T)	$\Gamma$ (mm/s)	Phase	Spectral contribution
Olivine untreated	1.12	2.92	–	0.30	Fe <sup>2+</sup> (olivine)	56% (D1)
	0.33	0	48.6	0.56	Fe <sup>3+</sup> (oct-MgFe <sub>2</sub> O <sub>4</sub> )	22% (S1)
	0.28	0	46.5	0.56	Fe <sup>3+</sup> (tet-MgFe <sub>2</sub> O <sub>4</sub> )	17% (S2)
	0.42	0.62	–	0.48	Fe <sup>3+</sup> ( $\gamma$ -Fe <sub>2</sub> O <sub>3</sub> )	5% (D2)
Olivine Ox 1 h	1.12	2.92	–	0.30	Fe <sup>2+</sup> (olivine)	49% (D1)
	0.34	0	47.8	0.61	Fe <sup>3+</sup> (oct-MgFe <sub>2</sub> O <sub>4</sub> )	20% (S1)
	0.29	0	44.7	0.61	Fe <sup>3+</sup> (tet-MgFe <sub>2</sub> O <sub>4</sub> )	12% (S2)
	0.42	0.66	–	0.51	Fe <sup>3+</sup> ( $\gamma$ -Fe <sub>2</sub> O <sub>3</sub> )	9% (D2)
Olivine Ox 1 h, Red 1 h	0.37	−0.14	50.4	0.35	Fe <sup>3+</sup> ( $\alpha$ -Fe <sub>2</sub> O <sub>3</sub> )	10% (S3)
	1.12	2.93	–	0.30	Fe <sup>2+</sup> (olivine)	56% (D1)
	0.46	0.70	–	0.43	Fe <sup>3+</sup> ( $\gamma$ -Fe <sub>2</sub> O <sub>3</sub> )	5% (D2)
	0.37	−0.12	47.2	0.90	Fe <sup>3+</sup> (Fe <sub>2</sub> O <sub>3</sub> )	12% (S3)
	0	0	32.4	0.33	Fe <sup>0</sup> (metallic)	27% (S4)

Sextuplet 3 can be attributed to hematite and the fourth sextuplet corresponds to metallic Fe.

The dominant contribution (56%) in the spectrum of the untreated olivine sample is a doublet with an isomer shift (IS) of 1.12 mm/s and a quadrupole splitting (QS) of 2.92 mm/s, attributed to Fe<sup>2+</sup> in the olivine structure [13]. About 40% of the Fe atoms are present as two magnetic sextuplets (S1 and S2) that can be attributed to Fe<sup>3+</sup> in octahedral and tetrahedral sites of the spinel structure of magnesioferrite (MgFe<sub>2</sub>O<sub>4</sub>) [12,26]. A small contribution (5%) of a doublet with IS = 0.42 mm/s, assigned to superparamagnetic maghemite ( $\gamma$ -Fe<sub>2</sub>O<sub>3</sub>), is also observed. This Fe<sup>3+</sup>-phase is known to form from the olivine structure, when olivine is oxidized in air in the range of 600–900 °C [20].

After the oxidation treatment at 750 °C for 1 h (Fig. 1b), more than half (51%) of the iron, is present in the form of free iron-oxides. 10% of the Fe atoms are present as a sextuplet with IS = 0.37 mm/s, QS = −0.14 mm/s and H (hyperfine field) = 50.4 T, values corresponding well with those reported for Fe<sup>3+</sup> in hematite ( $\alpha$ -Fe<sub>2</sub>O<sub>3</sub>) [10]. The spectral contribution of the doublet, originating from paramagnetic hematite increases slightly.

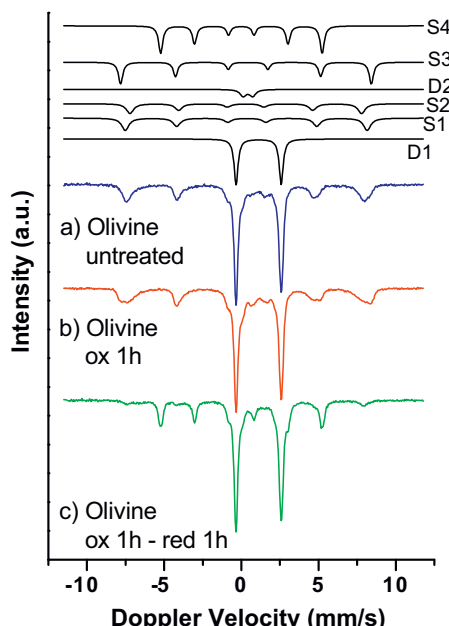


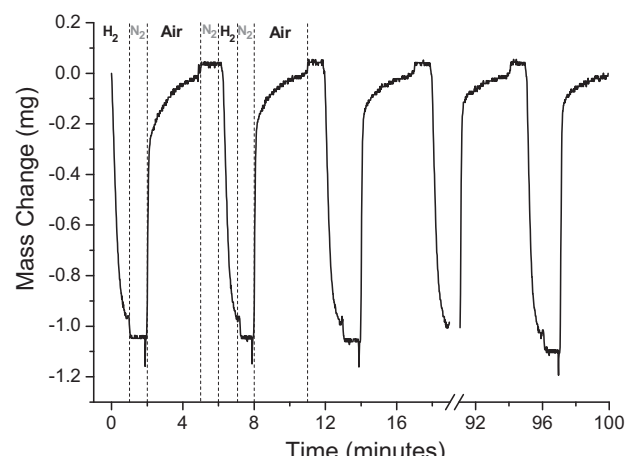
**Fig. 1.** Fitted <sup>57</sup>Fe Mössbauer spectra of the as received, untreated olivine (a), olivine which has been oxidized for 1 h (b) and olivine which has first been oxidized for 1 h and then reduced for 1 h (c). Subspectra of different components are indicated at the top.

After subsequent reduction (Fig. 1c), the dominating change is that 27% of the Fe is reduced to metallic Fe<sup>0</sup>. It is also evident that parts of the Fe<sup>3+</sup> species are reintegrated in the olivine structure as Fe<sup>2+</sup>, the initial olivine spectrum being recovered. The two sextuplets, originating from the magnesioferrite, have disappeared. The remaining Fe<sup>3+</sup> magnetic contribution can at least partially be assigned to hematite, while the presence of remnant magnesioferrite structures cannot be ruled out.

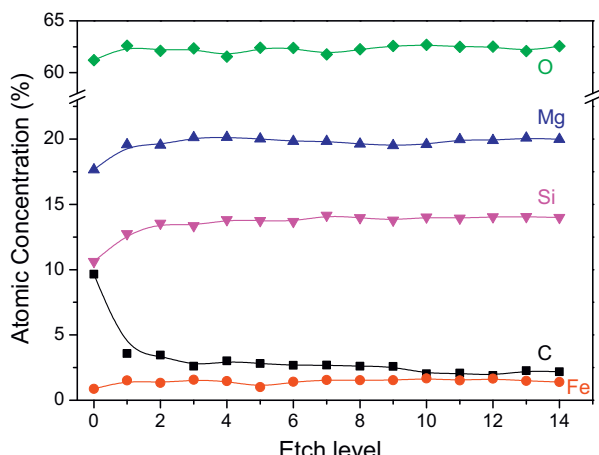
### 3.2. Thermo gravimetric analysis

Fig. 2 shows the results of the thermo gravimetric analysis (TGA) of an olivine sample under conditions simulating circulation between a gasification zone (reducing conditions) and an oxidation zone (oxidizing conditions) of an indirect gasification reactor. Oxidation and reduction times were chosen as 180 s and 60 s, respectively, to represent the conditions in an indirect gasifier with a riser reactor as the gasification zone and a bubbling fluidized bed as the oxidation zone, as applied in the MILENA process [27].

At time  $t=0$  min, the olivine was already oxidized in situ for 1 h at 750 °C. When the gas-environment was switched from oxidizing to reducing conditions, the mass of the sample decreased with 1 mg. After 60 s, the gas environment was switched back to oxidizing conditions and the mass of the sample reached its initial value after 180 s. In total 20 oxidation/reduction cycles were done, and the weight loss showed less than 2% difference during these 20 cycles. The apparent change in weight during the N<sub>2</sub> flush is a result of fluctuations in the gas flow rate and density and does thus



**Fig. 2.** Mass change of an 1 h pre-oxidized olivine sample (200 mg) during continuous oxidation (air, 180 s) and reduction (30% H<sub>2</sub>/He, 60 s) cycles at 750 °C, with intermediate N<sub>2</sub> flush.



**Fig. 3.** Atomic concentration of the elements present in untreated olivine, as a function of sample depth. Each etch level corresponds to approximately 35 nm sample depth.

not correspond to any change in weight of the sample material. The spikes just before and after flushing are also due to the switching of gas flows. This part of the experimental cycle is therefore not considered in the analysis.

The mass change during each cycle is a measure for oxygen transport. Since this change is 1.0 mg in each cycle and the amount of sample is 200 mg, the oxygen transport under these conditions amounts to 0.5 wt.%.

The mass changes during oxidation and reduction can be divided into two separate processes: (1) a very fast process, where 80% of the total mass change during the treatment is realized in just 5 s and (2) a slower, converging change of the mass with time, until the respective treatment is ended.

### 3.3. XPS

To study the composition of the outermost layers of olivine, XPS has been used in combination with depth profiling. Although XPS is a surface sensitive technique, which probes the first few nanometers of the sample, a depth profile can be obtained by combining a sequence of ion gun etch cycles with intermediate XPS analysis of the current surface.

Fig. 3 shows the depth profile of the untreated olivine. Apart from the elements present in olivine, Fe, Mg, Si and O, a significant amount of carbon is detected at the outer surface (etch level = 0).

This is due to carbonaceous contaminations, deposited on the sample during sample transfer under ambient conditions, which are frequently measured by XPS. The surface carbon is largely removed during the first ion gun etch. This results in an increase of the concentration of all other elements, indicating that the carbon was homogeneously distributed at the surface of the olivine. After further etching, the concentrations do not change significantly, which shows that the elemental composition of the untreated olivine is homogeneous as a function of sample depth.

Fig. 4 shows the depth profiles of oxidized and oxidized-reduced olivine. The concentration of the elements, present in olivine, is shown as a function of the etch level. When olivine is oxidized, the iron concentration at the surface (etch level = 0) increases significantly. When olivine is subsequently reduced, the iron concentration decreases again, to similar values as in the untreated olivine. XPS depth profiling yields valuable information on the dynamics of these surface layers.

After oxidation treatments, the concentration of iron decreases with increasing etch time. This shows that the iron is not homogeneously distributed throughout the sample, but that the surface of

the particle is richer in iron than the bulk. This iron enrichment is observed at two times scales; both for 1 min and 1 h of oxidation treatment. After oxidation for 1 h (solid red lines), the concentration of iron at the surface is increased to 5.8%. During several etching steps, the iron concentration decreases exponentially to a value of 2%. This corresponds to an iron rich layer of approximately 400 nm, where the iron concentration is twice as high as in the bulk, using the etch-rates in  $Ta_2O_5$  to convert the number of etch levels to a distance.

When the oxidized olivine is reduced for 1 min (dashed blue lines), the iron concentration at the surface decreases immediately to 3.6%. The depth profile shows that only the iron concentration close to the particle surface is affected by this short reduction. After three etching steps, the concentration resembles the respective iron concentration of the 1 h oxidized olivine. Longer reduction time (solid blue lines) results in a lower iron concentration, which is homogeneously distributed with respect to the sample depth. The amount of iron in these surface layers closely resembles the iron concentration on the surface of the untreated olivine.

Whereas the iron concentration at the surface increases upon oxidation, decreasing concentrations of Mg and Si are observed. The depth profiles show increasing concentrations of the latter two elements with prolonged etching. At increased sample depth, the Mg and Si concentrations are slightly larger compared to their bulk concentrations in the untreated olivine, indicated by the black dashed lines.

An interesting observation is that the concentrations of Fe and Si in the depth profiles appear to be each other's mirror image. This holds true, to a lesser extent, for the Mg and O concentrations as well.

Another observation is the difference between Mg and Si concentrations in the pre-oxidized, 1 min reduced sample (dashed blue lines), compared to the 1 h oxidized sample (solid red lines). The depth profiles of both samples have similar Mg concentrations with respect to sample depth. On the other hand, the silicon depth profile for the 1 min reduced sample looks markedly different from the 1 h oxidized one. After reduction of the pre-oxidized olivine for 1 min, the Si concentration at the surface is significantly higher than before this short reduction.

In other words, on the short time scale, Si is exchanged with Fe at the surface in the first stages of olivine reduction. In the longer run, Fe exchanges with Mg as well.

The depth profiles of the pre-oxidized, 1 h reduced sample show a significant decreased or increased surface concentration for Mg and O, respectively, compared to the concentrations at increased etching time.

An additional XPS depth profile study was carried out (see Fig. S1 in the Supplementary data) for a 1 h pre-oxidized olivine sample, after 20 oxidation-reduction cycles in the TGA, to check if the trends, presented in Fig. 4, are comparable after more oxidation-reduction cycles. The iron surface concentration was only marginally higher (6.5%), compared to the 1 h oxidized olivine (5.8%). All other elements also showed comparable distributions. This demonstrates that, although the sample which has undergone repeated redox cycles was exposed to air for an additional hour, the trends for the 1 h oxidized olivine, shown in Fig. 4, are also present when olivine has undergone repeated redox cycles.

Supplementary material related to this article found, in the online version, at <http://dx.doi.org/10.1016/j.apcatb.2013.01.041>.

## 4. Discussion

The results presented in this paper provide a great deal of information about changes in the phase composition of olivine treated

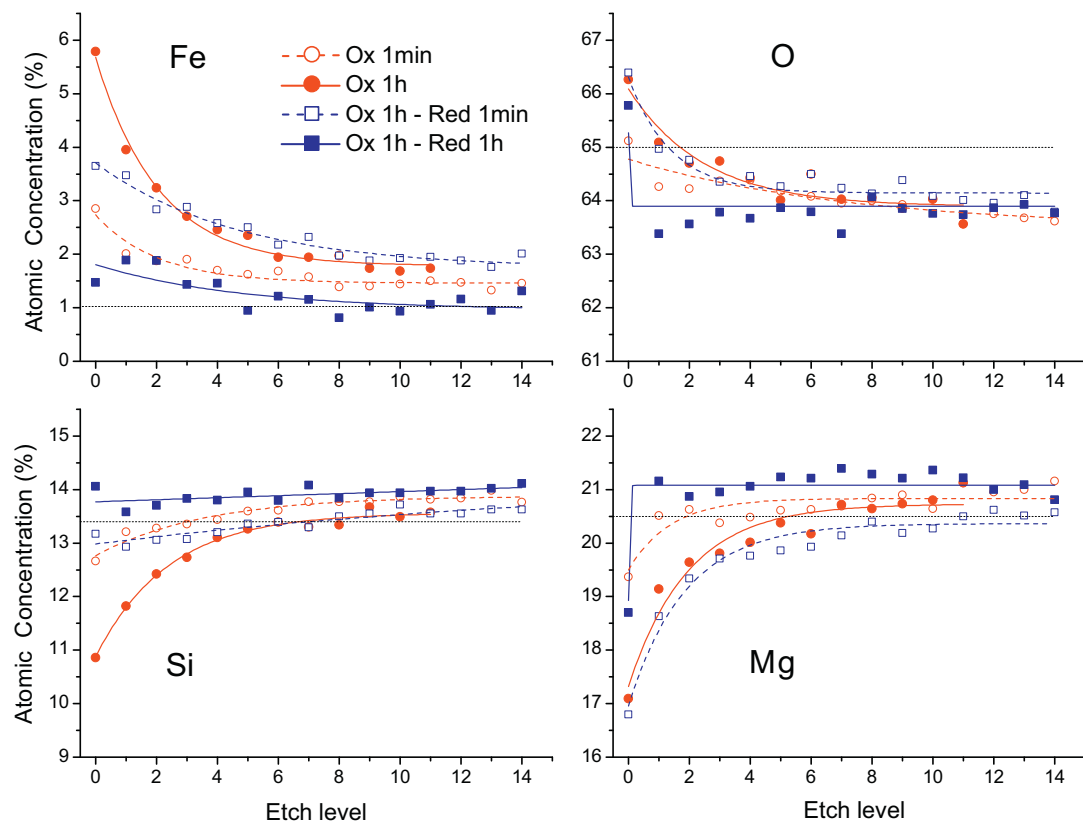


**Fig. 4.** Depth profiles of treated olivine samples. The concentration of the different elements is plotted as a function of sample depth. Treatments are as follows: 1 min oxidation, 1 h oxidation, 1 h oxidation followed by reduction for 1 min and 1 h oxidation followed by reduction for 1 h. The solid and dashed lines are exponential fits as a guide to the eye and the black dotted horizontal lines denote the bulk concentration of the respective elements in untreated olivine. Each etch level corresponds to approximately 35 nm sample depth.

in different gas environments. The combination of these three techniques, Mössbauer spectroscopy, TGA and XPS depth profiling gives unique insight into phase changes, both in space and time. In particular, the former two techniques give quantitative insight into the phase changes, whereas the latter provides information about sample homogeneity and spatial distribution of the elements.

#### 4.1. Oxygen transport

The TGA measurement (Fig. 2) can be used to determine the fraction of iron, actively participating in oxidation and reduction upon exposure to different gases. This determines the materials capability of transferring oxygen from the oxidation zone to the reduction zone. We assume that the near surface iron species, participating in these reactions, are  $\text{Fe}_2\text{O}_3$  and  $\text{Fe}^0$ . The assumption is based both on the results presented here and on previously reported XPS, XRD and Mössbauer analysis [10,12,23]. Although it is clear that full conversion of  $\text{Fe}_2\text{O}_3$  to  $\text{Fe}^0$  is not expected in a real system, using this assumption, a lower limit to the fraction of Fe that participates in the redox reactions can be determined. Moreover, we realize that pure  $\text{H}_2$  does not represent an industrial gas environment. However, the product gas of industrial scale indirect gasifiers consists of 40%  $\text{H}_2$  and 25% CO [14], which is very reductive as well. We chose  $\text{H}_2$  for our model study, because reduction by gases containing carbon gives unwanted side-effects, e.g. C-deposition.

The total mass change in each reduction/oxidation step is 1.0 mg. Since the used gases are free of contaminants, we assume that only addition or removal of oxygen causes this mass change. For the  $\text{Fe}_2\text{O}_3/\text{Fe}^0$  redox couple, 1.5 moles of atomic oxygen react with each mole of free Fe, or using the respective molar masses, 2.33 mg Fe for 1.0 mg of O. The absolute amount of iron in the sample is 12.6 mg

(200 mg sample with 6.3 wt.% Fe). With these numbers, it can be calculated that, under these conditions, 18.5% of all the iron present in olivine is participating in this redox process.

#### 4.2. Reversibility of phase changes

Results obtained by Mössbauer spectroscopy (Fig. 1 and Table 1) show that almost half (44%) of the iron in the (by us) untreated olivine is already driven out of the olivine matrix, through the pre-treatment applied by the mineral supplier. This free iron phase exists predominantly as the  $\text{Fe}^{3+}$  spinel structure of  $\text{MgFe}_2\text{O}_4$ . Despite the relatively low oxidation temperature of 750 °C, applied in our study, another 7% of Fe is extracted from the olivine matrix during oxidation treatment. A decreased spectral contribution of the spinel phase after oxidation is also observed. A simultaneous increase in the hematite phase indicates a conversion of the former two phases to the latter.

Previous research [12] shows that exclusion of Fe from olivine is significant at temperatures above 1100 °C. Taken into account that the mineral supplier already treated this olivine at 1600 °C for several hours, it may seem counter intuitive that additional Fe exclusion is observed at 750 °C. The 1600 °C pre-treatment was however done prior to grinding. During grinding, grain boundaries break up and fresh surfaces are created. These new surfaces are in direct contact with the surrounding gas environment. The observed phenomenon can thus be thought of as a surface effect.

Another important observation is that the extraction of iron out of the olivine matrix during oxidation is a reversible process; after reduction, the spectral contribution of the olivine phase is the same, 56%, as it was in the untreated material. However, the hematite phases and a significant amount of the iron present as spinel phase

are converted into metallic Fe<sup>0</sup> during reduction. This shows that there is only a partial reversibility of the phase composition upon reduction and that the material does not return to the untreated state.

#### 4.3. Sample homogeneity

The elemental concentrations in the untreated olivine, as a function of sample depth, as observed in XPS depth profiling (Fig. 3), show a homogeneous distribution of the constituting elements. This implies that the relative fraction of olivine and magnesioferrite is the same, throughout the bulk of the sample. Hence, the complete disappearance of the magnesioferrite upon reduction, as observed in Mössbauer spectroscopy, suggests that the phase changes are significant, also in the bulk of the material.

The observation that the untreated material is homogeneous, might at first glance seem to be in contradiction with our previous report, showing that the olivine is better regarded as a FeO<sub>x</sub>-catalyst, supported on Mg<sub>2</sub>SiO<sub>4</sub> and amorphous SiO<sub>2</sub>, than as a homogeneous material [23]. Different domains in olivine should indeed show different elemental concentrations up to the meso scale (1–100 μm). However, the XPS measurements are performed with a circular analysis area with a diameter of 400 μm. All elemental concentrations are averaged out over this area, resulting in homogeneous concentrations of the elements on this macro scale. However, after oxidation and reduction treatments, homogeneity is no longer observed in the direction perpendicular to the surface.

#### 4.4. Redox kinetics and diffusion

From the TGA-data, it is evident that the mass changes during oxidation and reduction can be divided into two separate processes; one fast, on the timescale of a few seconds and a slower, continuous process, on the timescale of several minutes. The results from XPS-depth profiling (Fig. 4) show a similar division into a fast and a slow process. The change in elemental composition of the surface layers, as a response to oxidizing and reducing gas treatments at 750 °C, differs both quantitatively and qualitatively for 1 min and 1 h treatments.

##### 4.4.1. Short term

The most obvious effect of the shorter treatments is a surface enrichment/depletion of Fe. After the oxidizing treatment, more Fe is observed at the surface, whereas a subsequent reduction quickly reduces the amount of surface Fe. After the 1 min treatments, only the upper surface layer of the material is affected, whereas changes in the bulk are insignificant. Fe increases/decreases predominantly at the expense of Si. We also observe that Fe species at the surface change oxidation state, from fully oxidized Fe<sup>3+</sup> to largely reduced Fe<sup>2+</sup>/Fe<sup>0</sup> state already after 1 min of reduction, in agreement with our previous study [23].

These observations, together with the fast mass changes observed with TGA, suggest oxidation/reduction of surface iron, excluded from Si-rich areas in the olivine. Iron oxide particles, present at the surface of the material, are in direct contact with the gas atmosphere and can therefore respond quickly to changes in the gas environment. The formation of iron oxide crystallites, supported on a Si-rich background, would show an increased presence of Fe at the expense of Si. As these iron oxide crystallites are reduced, their size will quickly decrease, thereby re-exposing Si at the surface.

Although the gas composition in a real gasification system will be less reducing than the gas used in our TGA measurements, our results show that olivine, and especially iron, is a very dynamic material on the time scale of seconds. With the changing oxidation state of iron, its catalytic properties change as well. Therefore,

different reactions will be catalyzed, depending on the catalysts residence time in the gasification zone. In particular, fast reduction of iron to its metallic state is beneficial for the removal of tars from the producer gas, since metallic iron catalyzes tar-cracking process conditions, relevant for biomass gasification [15,18].

Furthermore, the fast iron enrichment at fresh surfaces is an important observation in view of the use of olivine in fluidized-bed reactors. During use, the grain sizes will decrease, as a result of attrition, and new, fresh surfaces will be exposed to the gas environment. This attrition could actually result in a more active olivine, since more iron is quickly extracted from the olivine matrix to the surface when smaller particles are formed. The catalytically active surface area is hereby increased. Indeed, Rapagna et al. reported increasing H<sub>2</sub>-concentration in the product-gas as a function of time on stream, when untreated olivine was used as bed material [6], although it was not clear from their study whether this increase could be attributed to increasing iron surface area.

##### 4.4.2. Long term

The XPS depth-profiles show that changes in composition are largest at the surface, both in the long-term and in the short-term perspective. However, the long-term treatments influence the elemental composition in the entire probed depth of almost ~400 nm. After oxidation for 1 h, the iron concentration increases exponentially from the bulk to the surface of the particle. When the 1 h oxidized olivine is subsequently reduced, the iron-rich, upper layer is depleted. This results in a homogeneous iron concentration in the upper layers after 1 h of reduction, in line with the bulk concentration of the untreated olivine. In the long term, Fe increases/decreases at the expense of both Si and Mg. In addition, an increase/decrease in subsurface oxygen can be observed, inversely correlated to the Mg content.

Olivine is considered to be a non-porous material [7,12,21]. Therefore, reduction or oxidation of material inside the particles is likely to be diffusion limited, since gases cannot easily penetrate the solid particles. However, the complete conversion of the spinel MgFe<sub>2</sub>O<sub>4</sub> upon reduction in H<sub>2</sub>, together with the homogeneity of the untreated material, as observed with Mössbauer spectroscopy and XPS, respectively, suggest that the bulk of the material is affected as well as the surface. It is therefore likely that the slower changes, observed both in TGA and XPS, are due to diffusion limited reduction and oxidation reactions in the bulk of the material.

A plausible explanation for the ongoing bulk phase changes, in spite of the non porous nature of olivine, is the formation of cracks, caused by rapid morphological changes. Swierczynski et al. have observed that long, rodlike iron oxide precipitates are formed inside the olivine particles upon oxidation [12]. When this iron oxide reduces, it creates a hollow pore, or crack, inside the particle. These cracks have diameters up to several micrometers and make it possible for gases to migrate in and out of the particles. Moreover, Bleeker et al. have reported substantial internal self diffusion in iron oxide during continuous redox cycles, which seemed to speed up densification and internal sintering, causing cracks in the material [28].

The increase of Fe in the subsurface layer suggests a net migration of Fe toward the surface from the bulk of the material, presumably through defects in the crystal structure and/or at the surfaces of cracks and imperfections in the material, as discussed above. The simultaneous decrease in both Mg and Si content suggests that on the long-term, Fe migrates through both Fe- and Mg-rich domains of the material. Furthermore, the changes in the subsurface oxygen content shows that oxygen can migrate into and out of the material, but that this is a slow process.

A tentative explanation of the higher surface content of iron observed during oxidizing than during reducing conditions can be

found by considering the thermodynamics of the system. Calculations show that  $\text{Fe}_3\text{O}_4$ ,  $\text{SiO}_2$ , pyroxene and olivine are expected after treatment in oxidizing environments [29]. The same phases are expected under reducing conditions, with the exception that metallic Fe is expected instead of  $\text{Fe}_3\text{O}_4$ . Furthermore, the surface free energy of iron oxide is lower than that of metallic Fe [30,31]. Therefore, a larger energy gain is associated with bringing Fe to the surface during oxidizing conditions (as iron oxide) than during reduction (as metallic Fe). More Fe is thus expected at the surface under oxidizing conditions, as observed.

We also note the inverse correlation between O and Mg-content, especially at the outermost surface layer. This may be due to preferential oxidation/hydroxylation of Mg-rich domains in the material. Such an effect would help explaining the surprisingly low Mg surface content observed, both here and previously.

#### 4.5. Surface oxide formation

Finally, it should be noted that all measurements presented here were done ex situ. The samples were exposed to air upon transfer from the reaction chamber to each of the used analysis instruments. This is particularly important for the reduced samples. Even if these were completely reduced to  $\text{Fe}^0$  after the treatment, surface re-oxidation is to be expected in air at room temperature. It is therefore likely that, at least part of the  $\text{Fe}^{3+}$ , observed in the Mössbauer spectrum of the reduced sample, is due to an amorphous surface oxide. A surface oxide is indeed observed in the XPS-spectra of iron, even for the reduced samples. The iron in the depth profile of the reduced sample shows an oxide at the outer surface layer, but the iron in the inner layers is largely metallic. Surface oxides can also be seen from the sharp increase in the oxygen concentration at the surface. The excess oxygen is removed after one etching step, indicating that the surface oxide layer is thinner than 35 nm.

Analysis of the oxidation state of Fe-compounds from the depth profiles indicate sub-surface reduction of  $\text{Fe}_2\text{O}_3$  to  $\text{Fe}_3\text{O}_4$  and even metallic Fe, which, for the oxidized samples, is in contradiction with the Mössbauer measurements. However, it is known that, during sputtering experiments, the oxidation state of iron decreases with increasing etching time [32,33] due to preferential sputtering of the oxygen atoms. Therefore, we refrain from any in-depth analysis of Fe-oxidation states from these measurements.

## 5. Conclusion

We have used various characterization tools in order to investigate the capability of Austrian olivine to transport oxygen. This material is frequently used as a reactive bed-material in indirect biomass gasification.

Mössbauer spectroscopy confirmed that in the investigated Austrian olivine, almost half of the iron exists in the form of free iron oxides. Oxidation at 750 °C increases the content of free iron oxide phases from 44 to 51%. Part of the iron oxide phases reduce to metallic iron upon reduction, but a small fraction is reintegrated back into the  $\text{Fe}^{2+}$  phase of olivine.

TGA showed that olivine can transport 0.5 wt.% of oxygen and that the material is oxidized and reduced on two distinctly different time scales. The fast process is responsible for 80% of the mass changes and is attributed to surface oxidation/reduction. It was estimated that 18.5% of all the iron present in olivine contributes to the oxygen transport on time scales of one to several minutes.

XPS depth profiling showed that upon oxidation, a ~400 nm thick iron rich surface layer is formed. This iron enrichment is a reversible process; when oxidized olivine is reduced, the iron surface concentration decreases to similar values, as in the untreated

olivine. In similarity with the TGA results, elemental changes in the near surface region occur on two time scales. We attributed the fast process of Fe enrichment at the expense of Si, to oxidation of near surface Fe. The slower, sub surface process of Fe and O enrichment at the expense of Si and Mg is attributed to migration of the former two elements through the material.

Based on these results, it can be concluded that olivine transports a significant amount of oxygen on times scales, relevant for industrial processes. Changing process conditions influence the iron concentration at the surface and sub-surface layers. Hence, the oxygen transport capability, as well as the catalytic properties of olivine is heavily dependent on the process conditions, as these conditions determine the composition of olivine, especially in the near surface region.

## Acknowledgements

The authors would like to acknowledge Paul Hamers for his assistance with the TGA measurements. Funding from the Advanced Dutch Energy Materials Innovation Lab and the European Graduate School on Sustainable Energy is gratefully acknowledged.

## References

- [1] G.W. Huber, S. Iborra, A. Corma, Chemical Reviews 106 (2006) 4044–4098.
- [2] A.V. Bridgwater, Biomass and Bioenergy 38 (2012) 68–94.
- [3] D.A. Bulushev, J.R.H. Ross, Catalysis Today 171 (2011) 1–13.
- [4] N.L. Panwar, R. Kothari, V.V. Tyagi, Renewable & Sustainable Energy Reviews 16 (2012) 1801–1816.
- [5] T. Damartzis, A. Zabaniotou, Renewable & Sustainable Energy Reviews 15 (2011) 366–378.
- [6] S. Rapagna, N. Jand, A. Kiennemann, P.U. Foscolo, Biomass and Bioenergy 19 (2000) 187–197.
- [7] J.N. Kuhn, Z. Zhao, L.G. Felix, R.B. Slimane, C.W. Choi, U.S. Ozkan, Applied Catalysis B: Environmental 81 (2008) 14–26.
- [8] F. Miccio, B. Piriou, G. Ruoppolo, R. Chrione, Chemical Engineering Journal 154 (2009) 369–374.
- [9] S. Koppatz, C. Pfeifer, H. Hofbauer, Chemical Engineering Journal 175 (2011) 468–483.
- [10] M. Virginie, J. Adánez, C. Courson, L.F. de Diego, F. García-Labiano, D. Niznansky, A. Kiennemann, P. Gayán, A. Abad, Applied Catalysis B: Environmental 121–122 (2012) 214–222.
- [11] D. Sutton, B. Kelleher, J.R.H. Ross, Fuel Processing Technology 73 (2001) 155–173.
- [12] D. Swierczynski, C. Courson, L. Bedel, A. Kiennemann, S. Vilminot, Chemistry of Materials 18 (2006) 897–905.
- [13] M. Virginie, C. Courson, D. Niznansky, N. Chaoui, A. Kiennemann, Applied Catalysis B: Environmental 101 (2010) 90–100.
- [14] F. Kirnbauer, V. Wilk, H. Kitzler, S. Kern, H. Hofbauer, Fuel 95 (2012) 553–562.
- [15] T. Nordgreen, T. Liliedahl, K. Sjöström, Fuel 85 (2006) 689–694.
- [16] J. Pecho, T.J. Schildhauer, M. Sturzenegger, S. Biollaz, A. Wokaun, Chemical Engineering Science 63 (2008) 2465–2476.
- [17] S. Rapagna, M. Virginie, K. Galucci, C. Courson, M. Di Marcello, A. Kiennemann, P.U. Foscolo, Catalysis Today 176 (2011) 163–168.
- [18] T. Nordgreen, V. Nemanova, K. Engvall, K. Sjöström, Fuel 95 (2012) 71–78.
- [19] A. Sarvaramini, F. Larachi, Fuel 97 (2012) 741–750.
- [20] K. Barcova, M. Mashlan, R. Zboril, P. Martinec, Journal of Radioanalytical and Nuclear Chemistry 225 (2003) 529–533.
- [21] L. Devi, M. Craje, P. Thüne, K.J. Ptasiński, F.J.J.G. Janssen, Applied Catalysis A: General 294 (2005) 68–79.
- [22] T. Pröll, K. Mayer, J. Bolhär-Nordenkampf, P. Kolbitsch, T. Mattisson, A. Lyngfelt, H. Hofbauer, Energy Procedia 1 (2009) 27–34.
- [23] H.O.A. Fredriksson, R.J. Lancee, P.C. Thüne, H.J. Veringa, J.W. Niemantsverdriet, Applied Catalysis B: Environmental 130–131 (2013) 168–177.
- [24] Z. Klencsár, Nuclear Instruments and Methods B 129 (1997) 527–533.
- [25] S. Noorman, F. Galucci, M. van Sint-Annaland, H. Kuipers, Industrial and Engineering Chemistry Research 49 (2010) 9720–9728.
- [26] G. Bond, C. Molloy, F.S. Stone, Solid State Ionics 101 (1997) 697–705.
- [27] C.M. van der Meijden, Development of the MILENA gasification technology for the production of Bio-SNG, PhD thesis, Eindhoven University of Technology, 2010.
- [28] M.F. Bleeker, S.R.A. Kersten, H.J. Veringa, Catalysis Today 127 (2007) 278–290.
- [29] U. Nitisan, Journal of Geophysical Research 79 (1974) 706–711.
- [30] X.-G. Wang, W. Weiss, Sh.K. Shaikhutdinov, M. Ritter, M. Petersen, F. Wagner, R. Schlögl, M. Scheffler, Physical Review Letters 81 (1998) 1038–1041.
- [31] S. Hong, Current Applied Physics 3 (2003) 457–460.
- [32] T. Yamashita, P. Hayes, Applied Surface Science 254 (2008) 2441–2449.
- [33] D.S. Petrovic, D. Mandriño, Materials Characterization 62 (2011) 503–508.